Dental Materials xxx (xxxx) xxx

Contents lists available at ScienceDirect

Dental Materials

journal homepage: www.elsevier.com/locate/dental

Exploring the influence of placing bi-directional E-glass fibers as protective layer under a CAD-CAM resin composite on the fracture pattern

C.M. Saratti [a,*], N. Scotti [b], A. Comba [b], J. Bijelic-Donova [c], T. Suchy [d], M. Abdelaziz [a], J.G. Leprince [a], G.T. Rocca [a]

[a] Division of Cariology and Endodontology, School of Dentistry, University of Geneva, Geneva, Switzerland
[b] Department of Surgical Sciences, Dental School, University of Turin, Turin, Italy
[c] Department of Prosthetic Dentistry and Stomatognathic Physiology, Institute of Dentistry, University of Turku, Lemminkäisenkatu 2, Turku, Finland
[d] Department of Composites and Carbon Materials, Institute of Rock Structure and Mechanics, Academy of Sciences of the Czech Republic, Prague, Czech Republic

ARTICLE INFO

Keywords:
Fiber-reinforced composite
CAD-CAM
Multi-layered composite restoration
Fractography

ABSTRACT

Objectives: To investigate the influence of the presence and position of bidirectional E-glass fibers under a CAD-CAM resin composite on the fracture pattern evaluated both after quasi-static mechanical loading and after fatigue.

Methods: Rectangular specimens (10 mm-long, 5 mm-large and 4.2 mm-thick) were prepared and divided into four groups (n = 30/group). The control group (C-Group) consisted of a 4.2 mm-thick layer of monolithic CAD/CAM resin composite resin (Cerasmart, GC). In the 3 other groups including the placement of a fiber layer (F-Groups), the CAD/CAM resin composite layer was reduced to 3-, 2- and 1-mm thickness (F3-, F2- and F1-Groups, respectively). Two bonded layers of bidirectional E-glass FRC (Dentapreg, ADM A.S.) were bonded underneath and a light-curable resin composite base (Gaenial Posterior, GC) was then added to reach a total thickness of 4.2 mm for all samples. In each group, half of the specimens (n = 15) were submitted to quasi-static mechanical loading to failure in a universal testing machine. The other half (n = 15) was subjected to cyclic isometric stepwise loading until failure or completion of 105000 cycles (5000 cycles at 500 N, followed by five stages of 20000 cycles at 750 N, 1000 N, 1250 N, 1500 N, and 1750 N). The data were analyzed by Weibull statistics for quasi-static loading, and by the Kaplan-Meier product limit estimation procedure after fatigue. All fractured specimens were studied using light and electron microscopy techniques, and the types of fracture were determined.

Results: For quasi-static mechanical loading, significant differences were observed for Weibull modulus and characteristic strength between groups, with values ranging from 10.8 to 22.4 for the former and from 2336.6 to 2974.7 for the latter. Also, survival after stepwise fatigue revealed statistically significant differences between groups ($p < 0.05$), the lowest values of cycles before failure being observed for F1-Group – Median = 61223 (50415; 65446) – as compared to the other groups – C-Group: Median = 89005 (86189; 98195); F3-Group: Median = 85198 (77279; 87860); F2-Group: Median = 89306 (87454; 97024). Both in quasi-static loading and after fatigue, the observation of fracture modes revealed major differences. While all fractures were vertical (split) in C-Group, the majority of the specimens in F-Groups presented some degree of horizontal deflection of the crack. In all deviated fractures, fractographic analysis confirmed a toughening effect of the fiber layer.

Significance: The present in vitro work tends to show that the fracture pattern of CAD-CAM resin composites is favorably affected by the presence and position of an underlying bidirectional E-glass fiber layer. The placement of E-glass fibers under a CAD-CAM resin composite may therefore represent an interesting strategy to reduce the risk of catastrophic restoration failure, which could be integrated in the development of the new generation of indirect materials, possibly in 3D-printing approaches.

* Correspondence to: Division of Cariology and Endodontology, Clinique universitaire de médecine dentaire, 19 rue Lombard, rue Michel-Servet, 1211 Genève, Switzerland.
E-mail address: carlo.saratti@unige.ch (C.M. Saratti).

https://doi.org/10.1016/j.dental.2023.09.003
Received 31 October 2022; Received in revised form 17 August 2023; Accepted 15 September 2023
Available online 19 September 2023

1. Introduction

Teeth with root canal treatment have been shown in a large population database to be associated with reduced tooth longevity as compared to teeth without root canal treatment. [1] Moreover, most of root canal treated teeth have been reported to be lost due to non-restorable fracture. [2–4] The restoration of these teeth must therefore be designed with the aim of reducing the risk of such fractures.

Restorative concepts for endodontically treated teeth (ETT) have evolved in the last two decades and currently, endocrowns and overlays are considered as good alternatives to conventional post-core-crowns. [5] The in-vitro performance of these kind of restorations in terms of quasi-static mechanical resistance, fatigue resistance and adhesive retention are comparable to those of traditional prosthodontic solutions. [6,7] Moreover, results of clinical trials have also demonstrated good clinical performances of these adhesive post-free restorative strategies. [8,9].

The main concern remains the reduction of the risk of non-restorable fractures below the cemento-enamel junction. The crack, which usually originates on the occlusal surface of the restoration, can indeed travel through the restoration and then propagate into adjacent dental tissues, leading to unrepairable root fractures [10].

In order to prevent that, several authors have suggested that reinforcing the monolithic CAD/CAM resin composite restoration with a base of Fiber-Reinforced Composites (FRCs), especially glass fibers, could overcome this problem.[11,12] FRC materials exhibit superior mechanical properties compared to conventional particulate filled resins (PFRs)[13] and have the potential to interfere with the propagation of the fracture better than PFRs, due to their different and more efficient toughening mechanism.[14] Especially, FRCs containing long continuous fibers have shown superior tensile strength and toughness compared to short discontinuous FRCs, due to the high aspect-ratio and uniform alignment against stress (anisotropy).[15] Multiple ultra-thin sheets of continuous uni/bi-directional E-glass fibers can be packed and placed above the direct resin composite base in the case of overlays or endocrowns, or above the resin composite build-up beneath crown [16].

Despite the large number of studies available on FRC materials, there have been a few studies that have investigated aspects concerning this restorative approach. Generally, information on the behaviour of FRCs under fatigue stresses is still scarce. In fact, a load-to-fracture test should not be used alone to predict the mechanical behaviour of materials, as clinically restorations are known to fail in fatigue conditions under cyclic loadings.[17] Moreover, It has been shown that for brittle materials (as resin composite), a linear relationship exists between the thickness of a resin composite restoration and the strain needed to break it.[18] Tiu et al. investigated how the variations in thickness of the PFR veneering layer affect the toughness of the bi-layer short FRC/PFR systems [19]. Authors found that the specific work of fracture was optimal with maximum short-FRC thickness, while the thickness of the conventional PFR cover layer did not affect the toughness potential. Unlike short FRCs, whose consistency is very similar to PFRs, the extremely low thickness of long fiber networks (0.06 mm) limits their handling during clinical applications and, therefore, their final volume fraction is limited to 2–3 sheets of fibers.

Therefore, this study aimed to study the influence of the presence and position of a bilayered bidirectional E-glass FRC in structures composed of CAD/CAM resin composite as overlayer and particulate filled resin composite (PFR) as substrate, defining their fatigue resistance, quasi-static load-bearing capacity and fracture mode. The null hypotheses tested was that the presence and position of bidirectional E-glass fibers under a CAD-CAM resin composite had no influence on the fracture pattern evaluated both after quasi-static mechanical loading (maximum load) and after fatigue (number of cycles), including the type of fracture observed in both test modalities.

2. Materials and methods

2.1. Specimen preparation

Materials used in this study are listed in Table 1. A total of 90 specimens were fabricated (10 mm × 5 mm x 4.25 mm) by placing a 0.25 mm thick bidirectional FRC layer between a superficial layer of the CAD/CAM resin composite and a PFR substructure at different levels. In this bilayer structure, the CAD/CAM layer is simulating the coronal restoration and a PFR substructure is simulating the resin composite core build-up of an ETT. Unreinforced CAD/CAM resin composite specimens (n = 30) were made as control. The CAD/CAM resin composite blocks (Cerasmart, GC) were cut with a water-cooled low-speed diamond saw into slices with a thickness of 4.25 mm (n = 30, C-Group, control), 3 mm (n = 30, F3-Group), 2 mm (n = 30, F-Group), and 1 mm (n = 30, F1-Group). PFR substructures were fabricated by placing a conventional light-curable PFR (G-aenial Posterior, GC) into three silicon moulds (10 mm × 5 mm) to obtain slices with a thickness of 1 mm (n = 30), 2 mm (n = 30), and 3 mm (n = 30). The resin composite was horizontally stratified, and each increment of 1 mm was polymerized for 20 s using a second-generation LED high-power device with a power density of 1200 mW/cm^2 (Bluephase, Ivoclar-Vivadent). Then, two layers of continuous bidirectional E-glass fiber network (Dentapreg, UFM, ADM A.S.) were bonded to the resin composite substructures. Before bonding, each FRC layer was embedded for 10 min in a light-curing single component adhesive resin (Heliobond, Ivoclar Vivadent), protected from light and dried. The thickness of a single sheet of FRC is 0.1 mm. Consequently, the final thickness of the FRC layer was estimated to be around 0.25 mm also considering the thin layer of adhesive resin. The bilayered specimens were fabricated by bonding the CAD/CAM pieces to the FRC covered PFR substrates according to the following procedure (Fig. 1). The surface of each CAD/CAM slice was sandblasted with 27 μm aluminium-oxide powder (2 bar pressure, 5 s) (Kavo EWL, Type 5423), rinsed and dried. It was then immediately treated with two layers of a pre-hydrolysed organic silane (Monobond Plus, Ivoclar-Vivadent) for 60 s and dried, and subsequently covered with one layer of light-curing adhesive resin (Heliobond, Ivoclar Vivadent), which was left uncured. The CAD/CAM resin composite slices were then seated over the FRC covered substructures, the resin excesses were removed, and the specimen surface was light-cured for 90 s. The margins between the different layers were immediately finished and polished using discs of decreasing grain size (Pop On XT, 3 M).

Each group was further divided into two subgroups (n = 15): subgroups Cs, F3s, F2s, and F1s were subjected to a quasi-static fracture test, while subgroups Cd, F3d, F2d, and F1d were subjected to cyclic fatigue test.

2.2. Quasi-static fracture test

Specimens of Subgroups “s” were subjected to a fracture strength evaluation in a universal testing machine (Instron, Model 1114, Instron Corp.). Each specimen was placed in a fixing device, and a vertical 90° compressive load was applied over the specimen in the centre of the CAD/CAM resin composite surface using a 3 mm diameter stainless ball. A foil of 40 μm (Bausch Articulating Paper Inc., Nashua, USA) was inserted between the loading rod and the restoration to reduce peak stresses at the contact points and to mark the contact area surfaces. The pressure on the ball indenter was enforced at a crosshead speed of 1 mm/min. Specimens were loaded until fracture, and the maximum breaking loads were recorded in Newtons (N).

2.3. Step-wise fatigue loading

Specimens of Subgroups "d" were subjected to a cyclic loading test with MTS Mini Bionix 858.02 servo hydraulic testing system (Mini Bionix II, MTS, Eden Prairie, MN, USA) according to a stepwise loading

Table 1
Materials used in the study and their mechanical properties.

Brand name (manufacturer)	Chemical composition *	E-modulus (GPa) *	Fracture Toughness K_{IC} (MPa$\sqrt{m}$) *	LOT NUMBER
G-aenial posterior (GC, Tokyo, Japan)	Hybrid composite with a combination of pre-polymerized resin fillers (Silica containing, Strontium and Lanthanoid containing) averaging 16–17 μm in size, and inorganic fillers (Fluoroaluminosilicate > 100 nm; Fumed silica < 100 nm). The matrix consists of a mixture of UDMA and dimethacrylate co-monomers	8.23	1.4	1211062
Dentapreg UFM (ADM A.S., Brno, Czech Republic)	Light-curing bidimensional mesh fiber material (thickness of 0,1 mm).	-	-	UFM_03–022013
StickRESIN (Stick Tech Ltd, Turku, Finland)	Light-curing resin. Components: Bis-MEPP & TEGDMA (≈ 99%); PDMAEMA (<1%).	4.1	-	121219I
Cerasmart (GC, Tokyo, Japan)	Force absorbing hybrid ceramic CAD/CAM Block. Bis-MEPP, UDMA, DMA (flexible nano ceramic matrix). Silica (20 nm) and barium glass (300 nm) nanoparticles.	7.4	2.2	1404211

Abbreviations: PMMA = Polymethyl methacrylate; Bis-GMA = Bysphenol A diglycidylether methacrylate; UDMA = Urethane dimethacrylate; TEGDMA = Triethylene glycol dimethacrylate; Bis-MEPP = 2,2-Bis (4-methacryloxypolyethoxyphenyl) propane; PDMAEMA = 2-(dimethylamino)ethylmethacrylate.
* manufacturer information

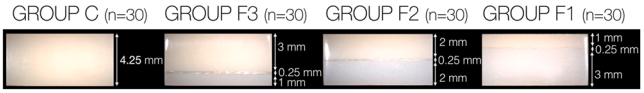

Fig. 1. Schematic representation of the experimental groups.

method. The specimens were loaded with a 3 mm diameter stainless steel ball and the fatigue test was carried out with unidirectional axial force. The isometric loading varied sinusoidally between a nominal peak value F and 10% of this value (R = 0.1). The loading frequency was 5 Hz. The test first started with 5000 cycles at 500 N as a warm-up load, followed by stages of 750, 1000, 1250, 1500, and 1750 N at a maximum of 20000 cycles each. The specimens were loaded until fracture or to a maximum of 105 000 cycles, and the number of endured cycles was registered. The peak/valley detector - a special MTS controller tool - was used during the test to evaluate the "health" of the specimen. This detector recognizes the difference between the current loading and the prescribed loading curve. A deviation is usually due to micro-fractures inside the specimen or to an accidental displacement.

2.4. Fractographic analysis

All fractured specimens were first analysed using a stereomicroscope (SZX9, Olympus optical Co. LTD) with magnification ranging from 6.3x to 50x and varying light angles. All detectable fracture surface features were photographed and recorded. Scanning Electron Microscopy (SEM) (Digital SEM XL20, Philips) was then used to analyse the fractured surfaces. For this purpose, all fragments were cleaned in an ultrasonic 10% sodium hypochlorite bath for 3 min, rinsed with water and dried. The specimens were then gold coated prior to the analysis. Magnifications up to 2000x were used to obtain high-definition images of the specific crack features in the selected areas of interest. The overall directions of crack propagation and failure origins were systematically mapped for all the fragments. Fracture patterns of all broken specimens were visually analysed and divided in three groups: split fracture, partially and totally deviated fractures. Classification was based on an agreement among three examiners.

2.5. Statistical analysis

The maximum breaking loads determined by the quasi-static fracture test were evaluated by the Weibull analysis (STATGRAPHICS Centurion XVII, StatPoint, USA). Weibull analysis was carried out according to the three-parametric distribution where the cumulative probability function is written such that the probability of failure (P_f) increases with the fracture stress variable:

$$(\sigma) \quad [T1]: P_f = 1 - \exp\left[-\left(\frac{\sigma - \sigma_u}{\sigma_\theta}\right)^m\right],$$

where m represents the Weibull modulus that describes the dispersion of the values (distribution shape parameter, the slope of the line), σ_u represents a minimum load bellow a test specimen will not break (threshold stress parameter), and σ_θ is the characteristic strength defined as the force at which 63.2% of the specimens will fail (scale parameter). In other words, the characteristic strength is the value of stress for which $\ln\left(\ln\left(1/\left(1-P_f\right)\right)\right)$ equals zero, and it is an analogue to the median strength.[20] The maximum likelihood method was used to estimate the Weibull distribution parameters assuming a 95% confidence level. The Weibull plot shows the failure probability versus force at failure (logarithmically scaled). A straight line on this plot, which corresponds to the fitted Weibull distribution, is plotted with the 95% confidence limits.

For the multiple sample comparison of mean values of the force at failure, a non-parametric analysis was employed because the assumption of homoscedasticity was violated and, subsequently, the Kruskal-Wallis test for multiple comparison with the subsequent post-hoc test based on the Bonferroni procedure. Statistical significance was accepted at $p \leq 0.05$.

The fatigue resistance of the four groups was compared using the Kaplan-Meier product limit estimation (Origin 2021, OriginLab, USA). At each time interval (defined by each load step), the number of specimens beginning the interval intact and the number of specimens fractured during the interval were counted, providing the probability of survival (%) at each load step. Plots of survivorship functions for each group were obtained. A Log-Rank test was used initially to determine if differences in the survival curves existed for the four experimental groups. Furthermore, a pairwise comparison was carried out in order to determine the differences amongst each pair of experimental groups. A Breslow (generalized Wilcoxon) test was used for this purpose. Statistical significance was accepted at $p \leq 0.05$.

3. Results

Table 2 summarizes the results of the quasi-static fracture test (Subgroup s), including the mean values of the load at failure, Weibull modulus (m), and characteristic strength (σ_θ). Monolithic CAD/CAM resin composite samples (Cs) had the highest values of load at failure. The results suggest that the maximum breaking force decreased linearly (R2 = 0.99) with decreasing CAD/CAM resin composite thickness. This decrease can be quantified as 22.1% (F1s), 12.5% (F2s) and 6.5% (F3s) compared to monolithic samples (Cs). Weibull analysis confirmed this

Table 2
Mean fracture load values (N), characteristic strength (S_0), and Weibull modulus (m) for group subjected to quasi-static fracture test.

Group	*n*	Force at failure (95% CI) [N]	m (95% CI)	σ_θ (95% CI)
Cs	*15*	2903.7 (2815.9; 2992.4)	22.4 (13.0; 30.4)	2974.7 (2895.6; 3055.8)
F3s	*15*	2716.8 (2546.5; 2886.6)	10.8 (6.2; 14.6)	2846.6 (2691.9; 3010.1)
F2s	*15*	2534.5 (2455.1; 2624.8)	17.7 (10.3; 24.0)	2611.7 (2524.3; 2702.0)
F1s	*15*	2263.9 (2170.2; 2356.2)	16.8 (9.7; 22.7)	2336.6 (2253.9; 2422.3)

finding (Table 2, Fig. 2), namely, a decreasing trend of the characteristic strength. While Weibull analysis revealed statistically significant differences among Groups Cs and F2s, F1s and F3s, and F2s and F1s, no statistical difference was found between Group F3s and the other groups. This can be explained by the relatively higher scatter in the data for Group F3s, which suggests a lower homogeneity of samples. This also corresponds to the calculated coefficients of variance, which were almost twice as high (11.3%) in the case of Group F3s.

After the stepwise fatigue loading, only two samples from Group Cd and one sample from Group F3d survived all 105000 cycles (1750 N loading phase). Specimens of all groups survived up to 45000 cycles (1000 N loading phase). The mean estimated cycles with confidence intervals were similar for the Groups Cd, F3d, and F2d (89005, 85198, and 89306, respectively), while the lowest values were observed in Group F1d (Table 3). The Kaplan-Meier curves (Fig. 3) showed the differences among all groups except for Cd-F2d (Breslow test, $p \leq 0.05$).

Modes of fracture were classified as shown in Table 4. All specimens in Group C fractured vertically (split fracture). In Groups F3 and F2, cracks were mainly partially deviated with few specimens showing split fracture after cyclic testing. In Group F1, the main fracture type was a totally deviated fracture for specimens fractured during the cyclic test, whereas a high heterogeneity was observed after the quasi-static load.

Fractographic analysis revealed important information about the crack propagation. The main origin of a split fracture (Fig. 4) was located at the occlusal surface from the major contact loading area underneath the loading ball, and the direction of crack propagation was always downwards. In partially deviated fractures (Fig. 5), the origins of the main fractures were located at the occlusal contact point, provoking downward median and cone fractures. However, secondary events extending upwards (radial cracks) were noticed at the interface between the CAD/CAM restoration and the FRC layer. This fracture pattern was frequent also in totally deviated fractures (Fig. 6). In the broken specimens of Subgroup F1d, fractures were mainly radial with an upward direction of propagation.

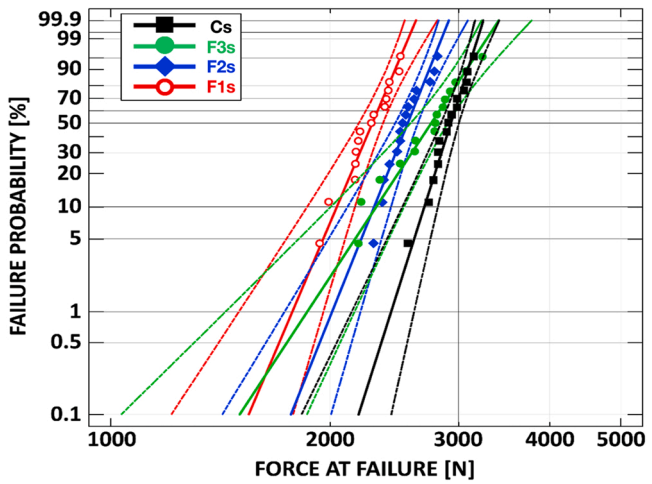

Fig. 2. Failure probability plots with Weibull analysis of the different groups.

Table 3
Pairwise post hoc comparisons with log rank test and medians for survival time.

Breslow	C	F3	F2	F1	medians of estimated cycles (95% CI)
C	x	p = 0.038	p = 0.862	p = 0.000	89005 (86189; 98195)
F3	p = 0.038	x	p = 0.021	p = 0.000	85198 (77279; 87860)
F2	p = 0.862	p = 0.021	x	p = 0.000	89306 (87454; 97024)
F1	p = 0.000	p = 0.000	p = 0.000	x	61223 (50415; 65446)

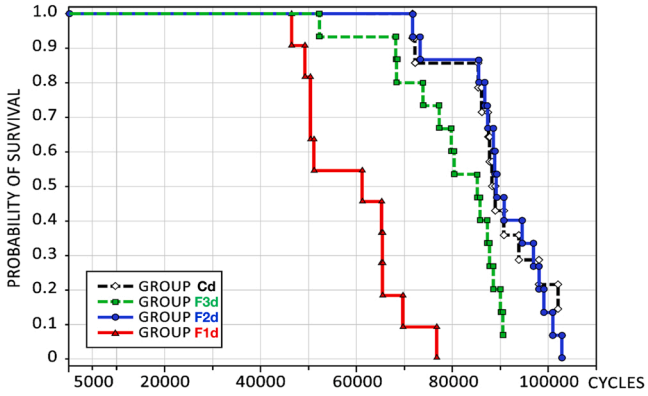

Fig. 3. Kaplan-Meier plotted survival curves of the experimental groups.

Table 4
Types of macroscopic failure for the experimental groups. In square brackets are marked the number of specimens with a mixed pattern of fracture, upward and downward cracks (Fig. 3a-d; Fig. 4a-d). In curved brackets are marked the number of specimens with a pure radial pattern of fracture with only upward cracks (Fig. 4e-h).

DEVIATION EFFECT	*GROUPS*							
	Cs	Cd	F3s	F3d	F2s	F2d	F1 s	F1 d
NO DEVIATION EFFECT (SPLIT	15	13	0	3	0	4	4	0
PARTIAL DEVIATION EFFECT	0	0	14	10	13	9 [5]	7[2]	1
TOTAL DEVIATION EFFECT	0	0	1	1	2 [2]	2 [2]	4 (2) [2]	14 (10) [4]
NO FRACTUIRE (in dynamic only)	-	2	-	1	-	0	-	0

4. Discussion

Null hypotheses were rejected since significant differences in fracture pattern and behaviour were observed both after quasi-static mechanical loading and after fatigue.

Regarding quasi-static mechanical tests, a Hertzian load-to-failure contact test with a spherical contact indenter over a flat-layer structure was used. This test allows simple, standardized, and reliable experimentation, clarifying the damage modes from initiation to final failure with minimal complications.[21] The Weibull analysis, which describes the resistance of a brittle material based on the survival probability, showed a uniform distribution and high homogeneity of the

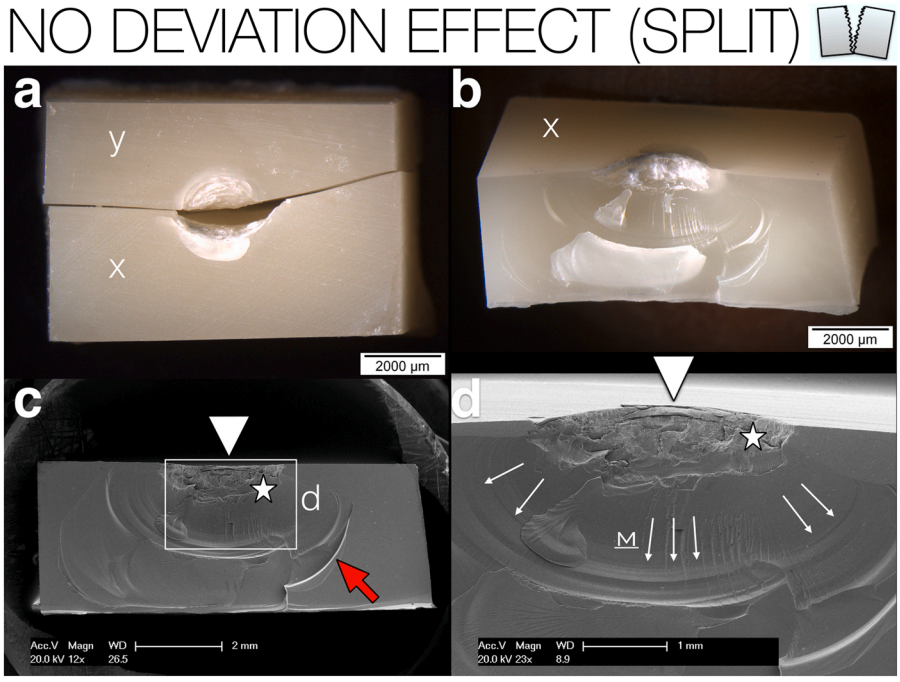

Fig. 4. Representatives images showing split medial fractures. (a) Occlusal view at the stereomicroscope of a specimen of Group Cd separated in two halves x and y. (b) Picture from the stereomicroscope of the fractured surface of fragment X. (c) Picture from the SEM of the fractured surface of fragment X. The white triangle indicates the main origin of the fracture; the white star marks the "quasi-plastic" damage zone; the red arrow marked an arrest line. (d) The fractured surface in higher magnification. White arrows indicate the direction of crack propagation, while underlined M indicates the fracture corresponding to a medial crack that started immediately beneath the quasi-plastic deformation area and propagated through the thickness of the specimen.

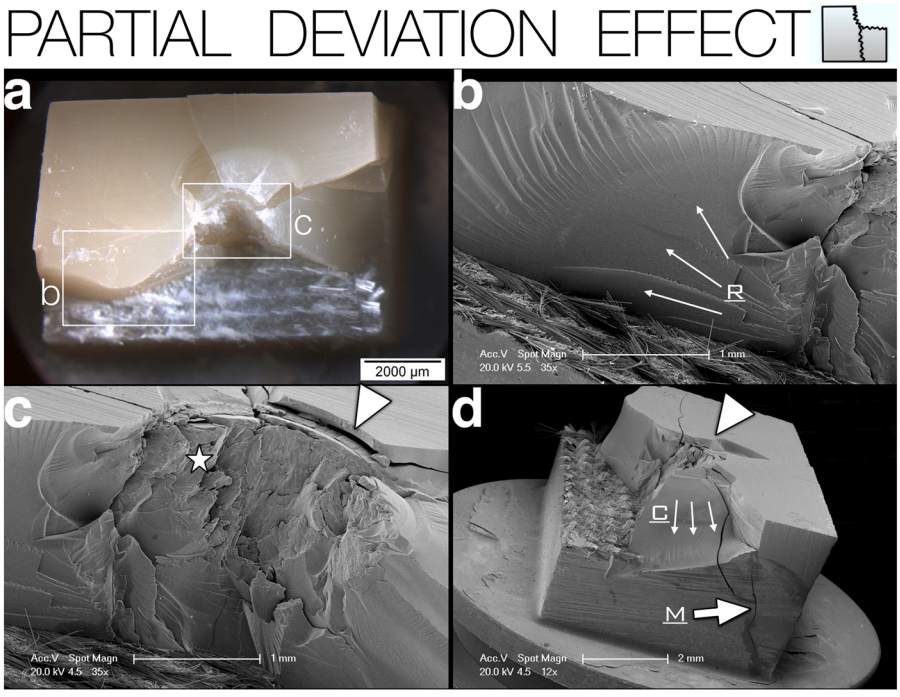

Fig. 5. Representatives images showing partially deviated fracture with mixed pattern (radial + medial and/or cone). (a) An occlusal view at the stereomicroscope of a specimen of Group F2s that presents multiple cracks. (b) Picture from the SEM of the fractured surface of the specimens. White arrows indicate the direction of crack propagation. On this crack plane, hackles clearly showed that the propagation was upward and outward, indicating that it was a radial crack (underlined R). (c) High magnification of the loading area. White triangle indicates the main origin of the fracture, while the white star marks the "quasi-plastic" damage zone; (d) Lateral view of the specimen. White arrows and an underlined C indicate the crack propagation of a cone crack; the white triangle indicates the origin of a medial downward crack that propagates through the layer of fiber, which is indicated by a big white arrow and an underlined M.

results, as was expected from the simplified model chosen as compared to a tooth model. Despite the fact that higher resistance values were measured for CAD/CAM resin composite layers, it must be highlighted that all values are greater than 2000 N, hence much higher than the normal physiological. However, the type of fracture put in evidence that the presence of the fiber layer has a certain potential to deflect the crack laterally, which is certainly interesting in an attempt to reduce the proportion of non-restorable tooth fracture.

Regarding fatigue testing, there are many aspects of fatigue failures that are unique from those caused by quasi-static loading. Firstly, failures typically occur at stresses typically happen at stresses significantly lower than those defined by ultimate strength, and leading to unforeseen failures that are not adequately predicted by measures of quasi-static strength. [22,23] Secondly, fatigue is a stochastic process that is dependent on the growth and coalescence of intrinsic flaws in the material. [24] This process is regarded as "stress-life fatigue" and is the most common mode of fatigue. [25] Under fatigue, statistically significant differences were observed in the number of cycles between the different subgroups, except between Groups F2d and Cd. Interestingly, a relatively distinct threshold could be observed. Specifically, the group of CAD/CAM resin composite with a thickness lower than 2 mm (Group F1d) displayed a notably lower cycle number (mean = 61223) compared

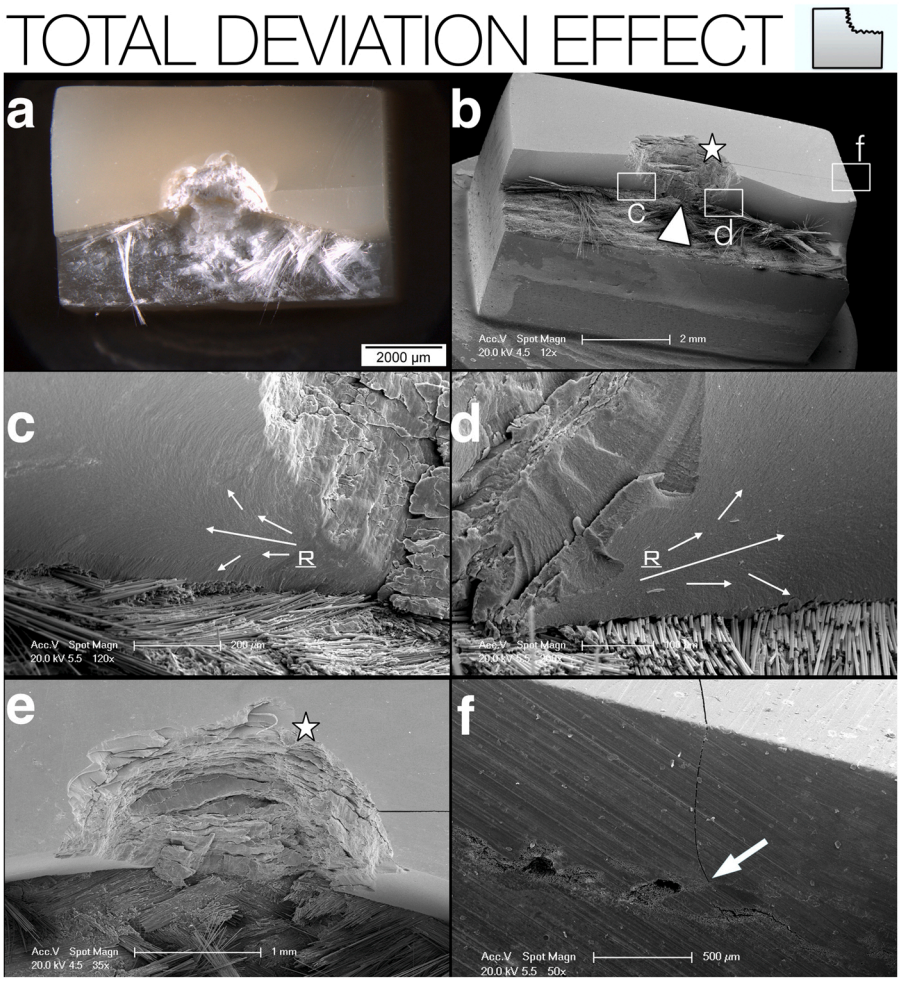

Fig. 6. Representatives images of a specimen where fracture did not propagate beneath the layer of fiber. (a) An occlusal view at the stereomicroscope of a specimen of Group F1d. (b) Picture from the SEM from another perspective. The white star marks the "quasi-plastic" damage zone; the white triangle indicates the origin of radial upward cracks. (c and d) High magnification of the fracture surface in the area between the damage zone and the FRC-CAD/CAM resin composite interface. White arrows indicate the direction of crack propagation. Hackles clearly showed that the propagation was upward and outward, indicating that it was a radial crack (underlined R). (e) an occlusal view of the contact area. White star marks the "quasi-plastic" damage zone. (f) A lateral view of the specimen at a high magnification. This secondary medial crack stopped at the level of the layer of fibers (white arrow).

to the other three groups which were in the same range (means ranging from to 85198–89306), albeit significant differences were still observed. Such an outcome is in line with the trend observed with quasi-static mechanical testing, with an increased resistance for thicker CAD/CAM resin composite layers. Moreover this is in agreement with a previous work, that reported a linear relationship between the thickness of the restorations and the load bearing capacity and fatigue resistance [26]. However, the results of the Group F2d does not fit in this general trend, since it resisted to a significantly higher number of cycles than the Group F3d. This may be explained by the placement of the fiber layer between equally thick layers of CAD/CAM and base resin composite materials (as in Group F2), resulting in a neutral axis that is located in the middle between the compression (CAD/CAM layer) and tension (base layer) side i.e. the stress is balanced. Typical for the neutral axis is that it moves along with the fiber layer. Consequently, if the fiber is placed more superficially (as in Group F1) or more deeply (as in Group F3), neutral axis is moved towards FRC layer and the remaining part of the restoration, below (Group F1) or above (Group F3) the fiber, is exposed to more tensile or more compressive stresses, respectively. Tensile stresses lead to fractures at lower loads, and compressive at higher loads. [27]. In accordance with the present finding, the existence of an optimum thickness of a superficial layer above a bidirectional FRC has been reported in previous work as 1.5–2.0 mm. [13,15] Furthermore, in the present investigation, the magnitude of stresses was also observed in the fracture of the fiber layer. In the group with balanced tensile and compressive stresses (Group F2, Fig. 5) the fiber layer deviated the crack, but it remained nearly intact. Conversely, in the group with higher tensile stresses in the lower part of the sample (within base resin composite layer) (Group F1, Fig. 6), the fracture has separated the two fiber layers, but stopped in the second layer, thus protecting the substrate. Also, Anton Y Otero et al. suggested that too deep placement of the fiber layer below massive endocrown restorations hinders its benefits, because of the too thick overlayer [28].

A quantitative comparison between Subgroup "s" and "d" was not possible because the load to failure test gave results in terms of Newton (N), while the stepwise fatigue test gave results in terms of numbers of cycles. However, a qualitative comparison between them was possible in terms of fracture mode in fractographic analysis. The analysis of fractures was carried out on all fragments to investigate the events that took place during the specimens' failure, combining stereo and scanning electron microscopy examination. Characteristic fractographic markers such as hackle lines, arrest lines, and wake hackle gave information on the origins and direction of crack propagation.[29,30] Groups Cs and Cd presented the same kind of fracture without any remarkable difference (Table 4); splitting in half of the specimens occurred systematically with the origin located on the upper surface corresponding to the contact load and with a vertical downward direction of crack propagation (Fig. 4). A zone of plastic permanent deformation was present beneath the main loading contact where the median crack was initiated. The tensile stress concentration below this zone leads to rapid microcrack coalescence, generating the ultimate crack. The main crack originated at the loading contact area and progressed downwards through the monolithic structure without interruption. Unlike what was observed for monolithic speciments (Group C), a stress breaker effect of the fiber layer provoking a deviation of the fracture, either partial or total (spalling), was found in 88% of the specimens reinforced with fibers, thereby confirming the

potential interest of interposing a fiber layer to potentially reducing the risk of non-restorable failure, which remains to be confirmed in a tooth-like model and in clinical studies. Groups F3 ("s" and "d") showed only a downward pattern of fractures (median and cone cracks). The mode of fracture mainly corresponded to a partially deviated, and descending cracks which were deviated at the interface between the CAD/CAM overlayer and the FRC layer. In Groups F2 ("s" and "d"), the mode of fracture was also mainly partially deviated. However, nine specimens presented a mixed downward (median and cone cracks) and upward (radial) pattern of fracture (Fig. 5). Median fractures resulted to be the main fracture pattern especially when concomitant with cone and radial cracks, with the latter always happening as secondary events. Lawn et al. investigated the fracture behaviour of monolithic and multilayer brittle structures subjected to Hertzian loads, emphasizing the role and the relationship of dissimilar E-modulus between layers. [31,32] When pure upward fractures (Fig. 4e-f) occurred, specimens failed because of a tensile stress located at the internal interface between the fiber layer and the upper CAD/CAM resin composite. The presence of radial cracks emphasises an area of augmented sub-surface tension due to the flexion of the upper resin composite layer over the softer FRCs. It is likely to speculate that the final E-modulus of the FRCs layer results from the combined properties of the bonding resin embedding the fiber nets and the latter. A defect inside the FRCs layer could have determinate the initiation of these localized cracks. [33] Such effect was not present in the specimens where the thickness of the CAD/CAM resin composite was higher than 2 mm.

In Group F1s, two specimens showed only radial cracks and the fracture was totally deviated. In this case, the radial crack also propagated perpendicular to the loading direction into the interface between the FRC and CAD/CAM resin composite layer, initiating the debonding of a large portion of the restoration and preserving the substructure. The above-mentioned damage competition between cone/median and radial cracks was more apparent in Group F1. In fact, the radial crack was the prevailing damage mode in the thinner CAD/CAM resin composite samples (Groups F1, "s" and "d") (Fig. 6). In Group F1s, radial cracks were detected in six specimens, while in Group F1d, they were detected in fourteen specimens. Moreover, in Group F1s, two fractures up to six were purely radial, while four were mixed; in Group F1d fractures of 10 specimens were purely radial.

The application of two different kinds of mechanical challenge had an impact on the mode of failure of the specimens. The amount of energy released during the progression of a fracture was significantly different if achieved under quasi-static and cyclic load. Quasi-static conditions resulted in a faster fracture propagation that carries a high amount of energy.[34] On the contrary, under cyclic loading, the mechanical degradation of the material leads to the expansion of subcritical flaws at subcritical charges. [35] The growth of such defect results in fractures that delivers a lower amount of energy due to their tendency to be deflected by an interface with a material with different properties rather than passing through it. Adhesive strength between interfaces also plays an important role. In order to obtain a stress-breaking effect in a structure with different materials such as PFRs and FRCs, the adhesion between the interfaces in a multilayer structure needs to be weak enough to prevent cracks from penetrating into the next layers (spalling or stopping), but strong enough to avoid delamination failures. [36] If the strength of the adhesion between interfaces is similar to the strength of the inter-filler adhesion of a resin composite, the structure will behave as if it is a monolithic, and the fracture will pass through the interface without any deviation. With a relatively strong interface, fracture energy might be absorbed by the substrate, allowing the crack to stop or deviate. If the adhesive bonding is weaker, delamination may occur. [37].

In summary, when median or cone cracks occur in a monolithic homogeneous material, they mainly generate split fractures. Radial cracks occur only in multilayer structures when the substructure is more elastic than the overlayer. In this case, the possibility of obtaining a stopping or spalling effect exists and it depends on the inner energy released by the propagation of the fracture and on the adhesive strength between the different interfaces. With strong energy and adhesion, the probability of obtaining a stopping or a deviation effect is low; with weaker energy and adhesion, the same probability is higher. [38,39].

Although this study has to be considered as a proof of concept regarding the potential interest of interposing a fiber layer under a CAD/CAM restoration, it has a clinical rationale. As mentioned earlier, restored ETT often fail because of unrestorable fractures, as was shown by large cohort studies.[4] Such fractures are often vertical root fractures, as illustrated by fractographic analysis of extracted teeth [10] Solutions to this problem may be kept in the fracture resistance mechanisms of intact vital teeth, where multiple cracks are always present in the enamel but they present remarkable resistance to propagation under high loads via several possible mechanisms [40,41], especially the role played by the dentin-enamel junction (DEJ). Since an interface as the DEJ does not exist in artificial restorative materials, the interposition of a layer of fibers as in the present work is a simple attempt to reproduce this structure. This bio-inspired concept has already been explored in the past with ~~some~~ interesting results. [42] Moving away from a tooth-like model, the present test which used superimposed flat layers was intended to serve as a proof of concept by providing a higher degree of standardization, which was confirmed by the low coefficient of variation of fracture strength values in all groups. Nevertheless, this methodology limits interpretation to rectangular specimens and would need to be reproduced in a tooth-like model in the future. Clinically, additional troubles for the accomplishment of this strategy may arise due to the difficulty of managing this extremely thin (0.1 mm) layer of fibers. Therefore, 3D-printing technologies may be used in the future to better implement such strategies [43].

5. Conclusions

Within the limits of this in-vitro study, the present work shows that the behaviour after fracture ~~pattern~~ of CAD-CAM resin composites is positively influenced by the presence and position of an underlying bidirectional E-glass fibers. However, a compromise depending on the position of the FRC must be considered: a more superficial position of the fiber layer led to an inferior performance of the restoration in terms of load bearing capacity and fatigue resistance, but a better stress breaking effect of the fiber was observed in terms of the mode of failure. In this case, the placement of E-glass fibers under a CAD-CAM resin composite may represent a valuable strategy to reduce the risk of catastrophic restoration failure.

Acknowledgments

The authors received no financial support and declared no potential conflicts of interest with respect to the authorship and/or publication of this article.

References

[1] Burke FJT, Lucarotti PSK. The ultimate guide to restoration longevity in England and Wales. Part 5: crowns: time to next intervention and to extraction of the restored tooth. Br Dent J 2018;225(1):33–48.
[2] Landys Borén D, Jonasson P, Kvist T. Long-term survival of endodontically treated teeth at a public dental specialist clinic. J Endod 2015;41(2):176–81.
[3] Axelsson P, Nyström B, Lindhe J. The long-term effect of a plaque control program on tooth mortality, caries and periodontal disease in adults. Results after 30 years of maintenance. J Clin Periodo 2004;31(9):749–57.
[4] Van Nieuwenhuysen JP, D'Hoore W, Leprince JG. What ultimately matters in root canal treatment success and tooth preservation: a 25-year cohort study. Int Endod J 2023;56(5):544–57.
[5] Rocca GT, Krejci I. Crown and post-free adhesive restorations for endodontically treated posterior teeth: from direct composite to endocrowns. Eur J Esthet Dent 2013;8(2):156–79.
[6] Rocca GT, Sedlakova P, Saratti CM, Sedlacek R, Gregor L, Rizcalla N, et al. Fatigue behavior of resin-modified monolithic CAD-CAM RNC crowns and endocrowns. Dent Mater 2016;32(12). e338-e50.

[7] Rocca GT, Daher R, Saratti CM, Sedlacek R, Suchy T, Feilzer AJ, et al. Restoration of severely damaged endodontically treated premolars: the influence of the endo-core length on marginal integrity and fatigue resistance of lithium disilicate CAD-CAM ceramic endocrowns. J Dent 2018;68:41–50.
[8] Belleflamme MM, Geerts SO, Louwette MM, Grenade CF, Vanheusden AJ, Mainjot AK. No post-no core approach to restore severely damaged posterior teeth: an up to 10-year retrospective study of documented endocrown cases. J Dent 2017;63:1–7.
[9] Al-Dabbagh RA. Survival and success of endocrowns: a systematic review and meta-analysis. J Prosthet Dent 2021;125(3). 415.e1-.e9.
[10] Saratti CM, Rocca GT, Durual S, Lohbauer U, Ferracane JL, Scherrer SS. Fractography of clinical failures of indirect resin composite endocrown and overlay restorations. Dent Mater 2021;37(6). e341-e59.
[11] Scotti N, Forniglia A, Tempesta RM, Comba A, Saratti CM, Pasqualini D, et al. Effects of fiber-glass-reinforced composite restorations on fracture resistance and failure mode of endodontically treated molars. J Dent 2016;53:82–7.
[12] Molnár J, Fráter M, Sáry T, Braunitzer G, Vallittu PK, Lassila L, et al. Fatigue performance of endodontically treated molars restored with different dentin replacement materials. Dent Mater 2022;38(4):e83–93.
[13] Garoushi S, Lassila LV, Tezvergil A, Vallittu PK. Load bearing capacity of fibre-reinforced and particulate filler composite resin combination. J Dent 2006;34(3):179–84.
[14] Vallittu PK. High-aspect ratio fillers: fiber-reinforced composites and their anisotropic properties. Dent Mater 2015;31(1):1–7.
[15] Garoushi S, Lassila LV, Tezvergil A, Vallittu PK. Static and fatigue compression test for particulate filler composite resin with fiber-reinforced composite substructure. Dent Mater 2007;23(1):17–23.
[16] Rocca GT, Rizcalla N, Krejci I. Fiber-reinforced resin coating for endocrown preparations: a technical report. Oper Dent 2013;38(3):242–8.
[17] Belli R, Geinzer E, Muschweck A, Petschelt A, Lohbauer U. Mechanical fatigue degradation of ceramics versus resin composites for dental restorations. Dent Mater 2014;30(4):424–32.
[18] Belli R, Wendler M, Zorzin JI, Lohbauer U. Practical and theoretical considerations on the fracture toughness testing of dental restorative materials. Dent Mater 2018;34(1):97–119.
[19] Tiu J, Belli R, Lohbauer U. Rising R-curves in particulate/fiber-reinforced resin composite layered systems. J Mech Behav Biomed Mater 2020;103:103537.
[20] Quinn JB, Quinn GD. A practical and systematic review of Weibull statistics for reporting strengths of dental materials. Dent Mater 2010;26(2):135–47.
[21] Lawn BR, Deng Y, Thompson VP. Use of contact testing in the characterization and design of all-ceramic crownlike layer structures: a review. J Prosthet Dent 2001;86(5):495–510.
[22] Arola D. Fatigue testing of biomaterials and their interfaces. Dent Mater 2017;33(4):367–81.
[23] Belli R, Petschelt A, Lohbauer U. Are linear elastic material properties relevant predictors of the cyclic fatigue resistance of dental resin composites? Dent Mater 2014;30(4):381–91.
[24] Kruzic JJ. Materials science. Predicting fatigue failures. Science 2009;325(5937):156–8.
[25] Yahyazadehfar M, Ivancik J, Majd H, An B, Zhang D, Arola D. On the mechanics of fatigue and fracture in teeth. Appl Mech Rev 2014;66(3):0308031–3080319.
[26] Rocca GT, Baldrich B, Saratti CM, Delgado LM, Roig M, Daher R, et al. Restoration's thickness and bonding tooth substrate are determining factors in minimally invasive adhesive dentistry. J Prosthodont Res 2021;65(3):407–14.
[27] Narva KK, Lassila LV, Vallittu PK. The static strength and modulus of fiber reinforced denture base polymer. Dent Mater 2005;21(5):421–8.
[28] Anton YOC, Bijelic-Donova J, Saratti CM, Vallittu PK, di Bella E, Krejci I, et al. The influence of FRC base and bonded CAD/CAM resin composite endocrowns on fatigue behavior of cracked endodontically-treated molars. J Mech Behav Biomed Mater 2021;121:104647.
[29] Scherrer SS, Lohbauer U, Della Bona A, Vichi A, Tholey MJ, Kelly JR, et al. ADM guidance-ceramics: guidance to the use of fractography in failure analysis of brittle materials. Dent Mater 2017;33(6):599–620.
[30] Scherrer SS, Quinn JB, Quinn GD, Wiskott HW. Fractographic ceramic failure analysis using the replica technique. Dent Mater 2007;23(11):1397–404.
[31] Lawn BRS, Zhang Y. Competing fracture modes in brittle materials subject to concentrated cyclic loading in liquid environments: bilayer structures. J Mater Res 2005;20(10):2792–800.
[32] Lawn BRS, Hermann I, Zhang Y. Competing fracture modes in brittle materials subject to concentrated cyclic loading in liquid environments: trilayer structures. J Mater Res 2006;21(2):512–21.
[33] Rocca GT, Saratti CM, Cattani-Lorente M, Feilzer AJ, Scherrer S, Krejci I. The effect of a fiber reinforced cavity configuration on load bearing capacity and failure mode of endodontically treated molars restored with CAD/CAM resin composite overlay restorations. J Dent 2015;43(9):1106–15.
[34] BR L. Fracture of brittle solids. Cambridge: Cambridge University Press.
[35] RO R. Mechanisms of fatigue-crack propagation in ductile and brittle solids. Int J Fract 1999;100(1):55–83.
[36] Chai HLB. Role of adhesive interlayer in transverse fracture of brittle layer structures. J Mater Res 2000;15(4):1017–24.
[37] Omran TA, Garoushi S, Lassila L, Shinya A, Vallittu PK. Bonding interface affects the load-bearing capacity of bilayered composites. Dent Mater J 2019;38(6):1002–11.
[38] Lawn BRDY, Miranda P, Pajares A, Chai H, Kim DK. Overview: damage in brittle layer structures from concentrated loads. J Mater Res 2002;17(12):3019–36.
[39] Jung YG, Wuttiphan S, Peterson IM, Lawn BR. Damage modes in dental layer structures. J Dent Res 1999;78(4):887–97.
[40] Chai H, Lee JJ, Constantino PJ, Lucas PW, Lawn BR. Remarkable resilience of teeth. Proc Natl Acad Sci USA 2009;106(18):7289–93.
[41] Lee JJ, Kwon JY, Chai H, Lucas PW, Thompson VP, Lawn BR. Fracture modes in human teeth. J Dent Res 2009;88(3):224–8.
[42] Monaco C, Arena A, Scotti R, Krejci I. Fracture strength of endodontically treated teeth restored with composite overlays with and without glass-fiber reinforcement. J Adhes Dent 2016;18(2):143–9.
[43] Saratti CM, Rocca GT, Krejci I. The potential of three-dimensional printing technologies to unlock the development of new 'bio-inspired' dental materials: an overview and research roadmap. J Prosthodont Res 2019;63(2):131–9.